



PCCP

Predicting ^1H NMR relaxation in Gd^{3+} aqua using molecular dynamics simulations

Journal:	<i>Physical Chemistry Chemical Physics</i>
Manuscript ID	CP-ART-07-2021-003356.R1
Article Type:	Paper
Date Submitted by the Author:	28-Aug-2021
Complete List of Authors:	Singer, Philip; Rice University, Chemical and Biomolecular Engineering Valiya Parambathu, Arjun; Rice University, Chemical and Biomolecular Engineering Pinheiro dos Santos, Thiago J.; Rice University, Chemical and Biomolecular Engineering Liu, Yunke; Rice University, Chemical and Biomolecular Engineering Alemany, Lawrence; Rice University, Chemistry Hirasaki, George; Rice University, Chemical and Biomolecular Engineering Chapman, Walter; Rice University, Chemical and Biomolecular Engineering Asthagiri, Dilipkumar; Rice University, Chemical and Biomolecular Engineering

SCHOLARONE™
Manuscripts



PCCP

Predicting ^1H NMR relaxation in Gd^{3+} aqua using molecular dynamics simulations

Journal:	<i>Physical Chemistry Chemical Physics</i>
Manuscript ID	CP-ART-07-2021-003356.R1
Article Type:	Paper
Date Submitted by the Author:	28-Aug-2021
Complete List of Authors:	Singer, Philip; Rice University, Chemical and Biomolecular Engineering Valiya Parambathu, Arjun; Rice University, Chemical and Biomolecular Engineering Pinheiro dos Santos, Thiago J.; Rice University, Chemical and Biomolecular Engineering Liu, Yunke; Rice University, Chemical and Biomolecular Engineering Alemany, Lawrence; Rice University, Chemistry Hirasaki, George; Rice University, Chemical and Biomolecular Engineering Chapman, Walter; Rice University, Chemical and Biomolecular Engineering Asthagiri, Dilipkumar; Rice University, Chemical and Biomolecular Engineering

SCHOLARONE™
Manuscripts

Journal Name

ARTICLE TYPE

Cite this: DOI: 00.0000/xxxxxxxxxx

Predicting ^1H NMR relaxation in Gd^{3+} -aqua using molecular dynamics simulationsPhilip M. Singer,^{*a} Arjun Valiya Parambathu,^a Thiago J. Pinheiro dos Santos,^a Yunke Liu,^a Lawrence B. Alemany,^b George J. Hirasaki,^a Walter G. Chapman,^a and Dilip Asthagiri,^{†a}Received Date
Accepted Date

DOI: 00.0000/xxxxxxxxxx

Atomistic molecular dynamics simulations are used to predict ^1H NMR T_1 relaxation of water from paramagnetic Gd^{3+} ions in solution at 25°C. Simulations of the T_1 relaxivity dispersion function r_1 computed from the Gd^{3+} - ^1H dipole-dipole autocorrelation function agree within $\simeq 8\%$ of measurements in the range $f_0 \simeq 5 \leftrightarrow 500$ MHz, without any adjustable parameters in the interpretation of the simulations, and without any relaxation models. The simulation results are discussed in the context of the Solomon-Bloembergen-Morgan inner-sphere relaxation model, and the Hwang-Freed outer-sphere relaxation model. Below $f_0 \lesssim 5$ MHz, the simulation overestimates r_1 compared to measurements, which is used to estimate the zero-field electron-spin relaxation time. The simulations show potential for predicting r_1 at high frequencies in chelated Gd^{3+} contrast-agents used for clinical MRI.

1 Introduction

The traditional theory of enhanced ^1H NMR (nuclear magnetic resonance) relaxation of water due to paramagnetic transition-metal ions and lanthanide ions in aqueous solutions originates from Solomon¹, Bloembergen and Morgan^{2,3}, a.k.a. the Solomon-Bloembergen-Morgan (SBM) model. The extended SBM model⁴ accounts for paramagnetic relaxation of inner-sphere water in the paramagnetic-ion complex¹⁻³, outer-sphere water^{5,6}, a.k.a. the Hwang-Freed (HF) model, the contact term^{2,3,7,8}, the Curie term^{9,10}, and the electron-spin relaxation^{3,9-15}. The extended SBM model is most widely used in the interpretation of paramagnetic enhanced ^1H relaxation of water due to Gd^{3+} -based contrast agents¹⁶⁻³⁸ used in clinical MRI (magnetic resonance imaging). The SBM model also forms the basis for the interpretation of paramagnetic relaxation in water-saturated sedimentary rocks³⁹⁻⁴⁶.

The inner-sphere water constitutes the ligands of the Gd^{3+} complex. The SBM inner-sphere model assumes a rigid Gd^{3+} - ^1H dipole-dipole pair undergoing rotational diffusion, which according to the Debye theory results in mono-exponential decay of the autocorrelation function. The Debye theory was previously used in the Bloembergen-Purcell-Pound (BPP) model⁴⁷ for like spins (e.g. ^1H - ^1H pairs), and then adopted in the SBM model for un-

like spins (e.g. Gd^{3+} - ^1H pairs). The SBM inner-sphere model also takes the electron-spin relaxation time into account, resulting in 6 free parameters for the ^1H NMR relaxivity r_1 . The inner-sphere relaxation is generally considered the largest contribution to relaxivity.

The outer-sphere water are less tightly bound than the inner-sphere water. The HF outer-sphere model assumes that the Gd^{3+} ion and H_2O are two force-free hard-spheres undergoing translational diffusion, which results in multi-exponential (i.e., stretched) decay of the autocorrelation function^{5,6}. The HF outer-sphere model adds an additional 2 free parameters, bringing the total to 8 free parameters for the extended SBM model. Relaxation from the contact term is negligible for ^1H NMR in Gd^{3+} -aqua^{23,31}, and is therefore neglected. Likewise, the Curie term is negligible in the present case^{9,10}.

The application of the SBM and HF models to Gd^{3+} -aqua therefore requires fitting 8 free parameters over a large frequency range in measured r_1 dispersion (NMRD). In chelated Gd^{3+} complexes, an order parameter plus a shorter correlation time^{48,49} are added to the rotational motion of the complex^{35,36}, or to the electron-spin relaxation^{22,30,33}, taking the total to 10 free parameters. This over-parameterized inversion problem often requires guidance in setting a range of values for the free parameters. It has also often speculated that the model for electron-spin relaxation is inadequate⁴.

Atomistic molecular dynamics (MD) simulations can help elucidate some of these issues. MD simulation were previously used for like-spins, e.g. ^1H - ^1H dipole-dipole pairs, such as liquid-state alkanes, aromatics, and water⁵⁰⁻⁵³, as well as methane over a

^a, Department of Chemical and Biomolecular Engineering, Rice University, 6100 Main St., Houston, TX 77005, USA

^b, Shared Equipment Authority and Department of Chemistry, Rice University, 6100 Main St., Houston, TX 77005, USA

^{*}, ps41@rice.edu

[†], dna6@rice.edu

large range of densities⁵⁴. In all these cases, good agreement was found between simulated and measured ^1H NMR relaxation and diffusion, without any adjustable parameters in the interpretation of the simulations. With the simulations thus validated against measurements, simulations can then be used to separate the intramolecular (i.e. rotational) from intermolecular (i.e. translational) contributions to relaxation, and to explore the corresponding ^1H - ^1H dipole-dipole autocorrelation functions in detail. For instance, MD simulations revealed for the first time ever that water and alkanes do not conform to the BPP model of a mono-exponential decay in the rotational autocorrelation function, except for highly symmetric molecules such as neopentane. More complex systems such as viscous polymers⁵⁵ and heptane confined in a polymer matrix⁵⁶ have also been simulated, which again saw good agreement with measurements, and which lead to insights into the distribution in dynamic molecular modes.

In this report, we extend these MD simulation techniques to Gd^{3+} - ^1H dipole-dipole pairs, i.e. unlike spins, in a Gd^{3+} -aqua complex. The simulations show good agreement with measurements in the range $f_0 \simeq 5 \leftrightarrow 500$ MHz, without any adjustable parameters in the interpretation of the simulations, and without any relaxation models. These findings show potential for predicting r_1 at high frequencies in chelated Gd^{3+} contrast agents used for clinical MRI, where $f_0 \simeq 64$ MHz (1.5 T) is the typical MRI operating frequency. At the very least, the simulations could reduce the number of free parameters in the SBM and HF models, and help put constraints on its inherent assumptions for clinical MRI applications.

The manuscript is organized in follows. Section 2 (Methodology) comprises sections 2.1 to 2.7, wherein we cover the simulation, bench-marking results that are essential to the methodology, and measurements. Section 3 (Results and discussions) comprising sections 3.1 to 3.4 is focused on the main aspect of this paper, namely NMR relaxation. Section 4 (Conclusions) provides the overall conclusions of this work.

2 Methodology

2.1 Molecular simulation

To model the Gd^{3+} -aqua system, we use the AMOEBA polarizable force field to describe solvent water⁵⁷ and the ion⁵⁸. The Gd^{3+} ion has an incomplete set of $4f$ orbitals, but this incomplete shell lies under the filled $5s$ and $5p$ orbitals. Thus ligand-field effects⁵⁹ are not expected to play a part in hydration and a spherical model of the ion ought to be adequate. However, polarization effects are expected to be important given the large charge on the cation.

Experimental NMR studies on Gd^{3+} -aqua use concentrations of about 0.3 mM. This amounts to having one GdCl_3 molecule in a solvent bath in a cubic cell about 176 \AA in size. Such large simulations are computationally rather demanding with the AMOEBA polarizable forcefield. Further, at such dilutions, the ions essentially “see” only the water around them, and since understanding the behavior of water around the ion is of first interest, here we study a single Gd^{3+} ion in a bath of 512 water molecules. (Note that within the Ewald formulation for electrostatic interactions, there is an implicit neutralizing background. This back-

ground does not impact the forces between the ion and the water molecules that are of interest here.) The partial molar volume of Gd^{3+} in water at 298.15 K has been estimated by Marcus (1985) to be -59.6 cc/mol . We use this to fix the length of the cubic simulation cell to 24.805 \AA . (From constant pressure simulations in a 2006 water system we find a Gd^{3+} partial molar volume of about -63 cc/mol , in good agreement with the value suggested by Marcus. However, in this work, we will use the value suggested by Marcus.)

All the simulations were performed using the OpenMM-7.5.1 package⁶⁰. The van der Waals forces were switched to zero from 11 \AA to 12 \AA . The real space electrostatic interactions were cut-off at 9 \AA and the long-range electrostatic interactions were accounted using the particle mesh Ewald method with a relative error tolerance of 10^{-5} for the forces. In the polarization calculations the (mutually) induced dipoles were converged to 10^{-5} Debyes.

The equations of motion were integrated using the “middle” leapfrog propagation algorithm with a time step of 1 fs coupled; this combination of method and time step provides excellent energy conservation in constant energy simulations. Exploratory work shows that the NMR relaxation in the Gd^{3+} -aqua system is sensitive to the system temperature. So we additionally use with a Nosé-Hoover chain^{61,62} with three thermostats⁶³ to simulate the system at 298.15 K. The collision frequency of the thermostat was set to 100 fs to ensure canonical sampling. We carried out extensive tests with and without thermostats to ensure that the Nosé-Hoover thermostat does not affect dynamical properties. Our conclusions are consistent with an earlier study on good practices for calculating transport properties in simulations⁶⁴.

Initially, the system was equilibrated under NVT conditions at 298.15 K for over 200 ps. We then propagated the system under the same NVT conditions for 8 ns, saving frames every 0.1 ps for analysis. We used the last 6.5536 ns of simulation (equal to $65536 (= 2^{16})$ frames) for analysis. The mean temperature in the production phase was 298.15 K with a standard error of the mean being 0.03 K.

2.2 Structure and dynamics

Fig. 1 shows the ion-water radial distribution function. The location and magnitude of the peak is in good agreement with earlier studies founded on either *ab initio*³¹ or empirical force field-based³³ simulations. Consistent with those studies, we find that the first sphere (i.e. inner sphere) contains between $q = 8 \leftrightarrow 9$ water molecules, with a mean of $q \simeq 8.5$ determined from $n_{\text{Gd-O}}(r)$ at $r \simeq 3.5 \text{ \AA}$. These values of q are consistent with the published range^{16,18,22,23,25,33,34}.

2.3 Residence time analysis

To estimate the residence time of water molecules in the inner sphere, we need to keep track of the water molecule as it moves into/out of the inner sphere. To this end, we follow the residence time of a defined water molecule w using an indicator function χ_w that equals 1 if the water molecule is in the inner sphere and zero otherwise. The inner sphere is defined as a sphere of radius

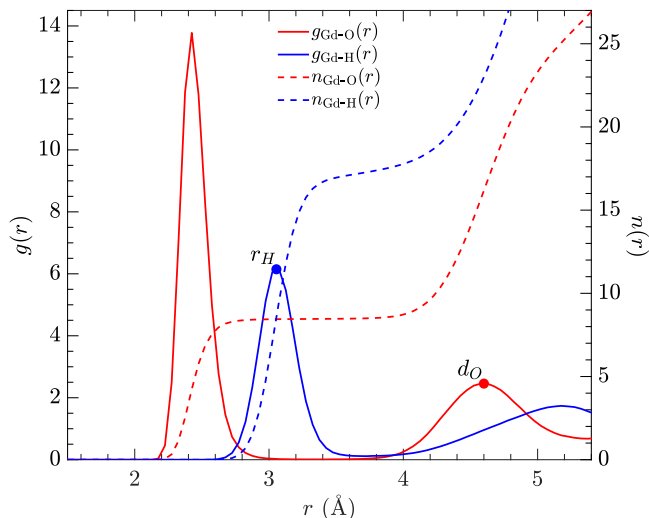


Fig. 1 Radial distribution function of water oxygen ($g_{\text{Gd-O}}(r)$) and hydrogen ($g_{\text{Gd-H}}(r)$) around the Gd^{3+} ion; the dashed lines are the corresponding coordination numbers $n_{\text{Gd-O}}(r)$ and $n_{\text{Gd-H}}(r)$. Also shown is the mode for $g_{\text{Gd-H}}(r)$ corresponding to Gd-H distance r_H for the inner-sphere, and the mode for $g_{\text{Gd-O}}(r)$ corresponding to Gd-O distance d_O for the outer-sphere.

$r \leq 3.3 \text{ \AA}$ around the Gd^{3+} ion; this corresponds to the first hydration of the ion (Fig. 1). We perform this analysis for all the water molecules that visit the inner sphere at least once during the simulation. (We emphasize that the time here is discrete because configurations are saved only every 100 fs.)

Fig. 2 shows the trace of the indicator function for a particular water molecule. Note that during the approximately 4 ns window (from the $\approx 8 \text{ ns}$ trajectory), the water molecule makes several excursions out of the inner sphere before permanently leaving the inner sphere around 4.5 ns. The length of time that the water molecule spends continuously inside the inner sphere is denoted by τ_i . As Fig. 2 shows, there can be several such islands of continuous occupation.

To test if the transient excursion is a bona fide escape from the inner sphere, we window average the data as follows: we consider a transient escape as a bona fide escape only if it persists for a defined number of consecutive time points. Fig. 2 shows the trace (blue curve) for such a “windowing” for a window length of 200 fs, i.e. two consecutive frames in the trajectory of configurations. As can be expected, windowing extends the length of time that the molecule is defined to be inside the inner sphere.

For all the water molecules that visit the inner sphere, we accumulate the set $\{\tau_i\}$ and then construct the histogram $h(\tau)$. Fig. 3 shows the $h(\tau)$ for the raw data and the data with window length of 200 fs. The $h(\tau)$ curve shows that there are many cases where water only transiently resides in the inner sphere. But we also find several water molecules that spend upwards of 0.5 ns continuously within the inner sphere. Specifically, for the data that has not been smoothed by “windowing”, we find three instances of water molecules continuously spending between 1 to 1.5 ns inside the inner sphere (and these also happen to be three distinct water molecules [data not shown]); with windowing using

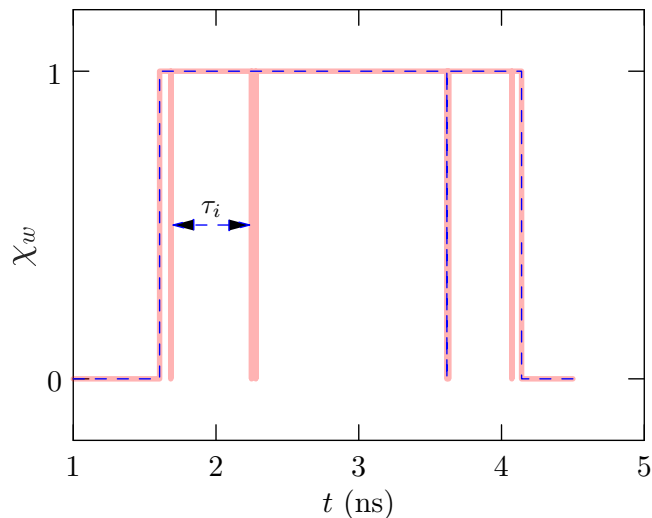


Fig. 2 The trace of the indicator function χ_w for part of the simulation trajectory (red curve). Note the several transient escapes of the water molecule out of the inner sphere. The dashed (blue) curve is obtained by “windowing” the raw data as noted in the text. τ is the length of time the water molecule spends continuously inside the inner sphere (one such domain, τ_i , is shown).

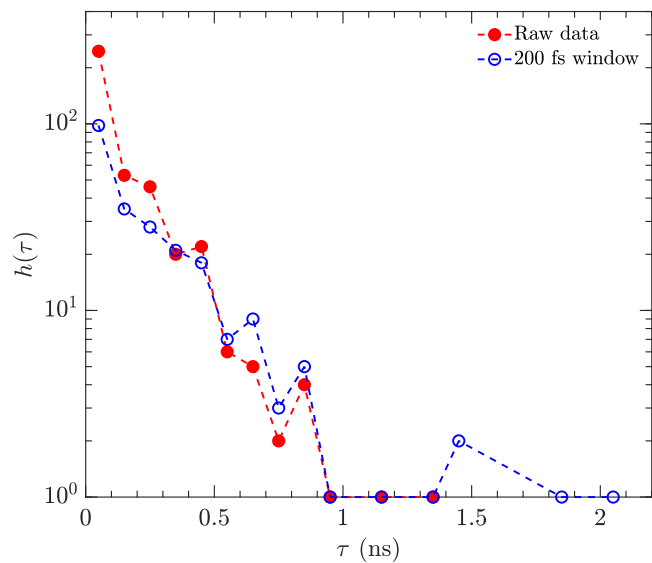


Fig. 3 Distribution of continuous occupancy times τ , $h(\tau)$, for raw data and 200 fs window.

a 200 fs window, the upper limit is extended to just over 2 ns. Thus residence time, τ_m , between $1 \leftrightarrow 2 \text{ ns}$ are predicted for a complete rejuvenation of the inner sphere population. This timescale is in accord with the range of published ^{17}O NMR data that suggest residence times $\tau_m \simeq 1.0 \leftrightarrow 1.5 \text{ ns}$ ^{17,21,28,65,66}.

2.4 ^1H NMR relaxivity

The enhanced ^1H NMR relaxation rate $1/T_1$ for water is given by the average over the $N = 1024$ ^1H nuclei in the $L = 24.805 \text{ \AA}$ box

containing one paramagnetic Gd^{3+} ion:

$$\frac{1}{T_1} = \frac{1}{N} \sum_{i=1}^N \frac{1}{T_{1i}}, \quad (1)$$

$$\frac{1}{T_2} = \frac{1}{N} \sum_{i=1}^N \frac{1}{T_{2i}}, \quad (2)$$

where T_{1i} is the T_1 relaxation for the i 'th ^1H nucleus. The gadolinium molar concentration is given by $[\text{Gd}] = [\text{H}]/N$, where $[\text{H}]$ is the molar concentration of ^1H in the simulation box. Equivalently, $[\text{H}] = 2[\text{W}]$ where $[\text{W}] = 55,705 \text{ mM}$ is the molar concentration of H_2O at 25°C . This leads to the following expression for the relaxivity in units of $(\text{mM}^{-1}\text{s}^{-1})$:

$$r_1 = \frac{1}{[\text{Gd}]} \frac{1}{T_1} = \frac{1}{[\text{H}]} \sum_{i=1}^N \frac{1}{T_{1i}}, \quad (3)$$

$$r_2 = \frac{1}{[\text{Gd}]} \frac{1}{T_2} = \frac{1}{[\text{H}]} \sum_{i=1}^N \frac{1}{T_{2i}}. \quad (4)$$

Note that $r_{1,2}$ are independent of N (or box size L , equivalently). The "fast-exchange" regime ($T_{1,2} \gg \tau_m$) is assumed¹¹, and the chemical shift term in r_2 ¹⁰ is neglected for simplicity. Note also that the ^1H - ^1H dipole-dipole relaxation⁵⁰ is not considered in these simulations.

The computation of $T_{1i,2i}$ originates from the Gd^{3+} - ^1H dipole-dipole autocorrelation function $G(t)$ ^{5,47,67-70} shown in Fig. 4(a), where t is the lag time. This autocorrelation is well suited for computation using MD simulations^{71,72}. Using the convention in the text by McConnell⁶⁸, $G_i(t)$ in units of (s^{-2}) is determined by:

$$G_i(t) = \frac{1}{4} \left(\frac{\mu_0}{4\pi} \right)^2 \hbar^2 \gamma_I^2 \gamma_S^2 S(S+1) \times \left\langle \frac{(3 \cos^2 \theta_i(t+t') - 1)}{r_i^3(t+t')} \frac{(3 \cos^2 \theta_i(t') - 1)}{r_i^3(t')} \right\rangle, \quad (5)$$

for the i 'th ^1H nucleus. θ_i is the angle between the Gd^{3+} - ^1H vector \mathbf{r}_i and the applied magnetic field \mathbf{B}_0 . μ_0 is the vacuum permeability, \hbar is the reduced Planck constant. $\gamma_I/2\pi = 42.58 \text{ MHz/T}$ is the nuclear gyro-magnetic ratio for ^1H with spin $I = 1/2$, and $\gamma_S = 658 \gamma_I$ is the electron gyro-magnetic ratio for Gd^{3+} with spin $S = 7/2$.

Note that in Eq. 5 we assume a spherically symmetric (i.e. isotropic) system, and therefore $G_i^m(t) = G_i(t)$ is independent of the order m , which amounts to saying that the direction of the applied magnetic field $\mathbf{B}_0 = B_0 \mathbf{z}$ is arbitrary. This assumption was verified in Ref.³³. For simplicity, we therefore use the $m = 0$ harmonic $Y_2^0(\theta, \phi) = \sqrt{5/16\pi} (3 \cos^2 \theta - 1)$ for the MD simulations⁵⁰.

The second-moment $\Delta\omega_i^2$ (i.e. strength) of the dipole-dipole interaction is defined as such⁶⁹:

$$G_i(0) = \frac{1}{3} \Delta\omega_i^2. \quad (6)$$

Assuming the angular term in Eq. 5 is uncorrelated with the distance term at $t = 0$, the relation $\langle (3 \cos^2 \theta_i(\tau) - 1)^2 \rangle_\tau = 4/5$ (which

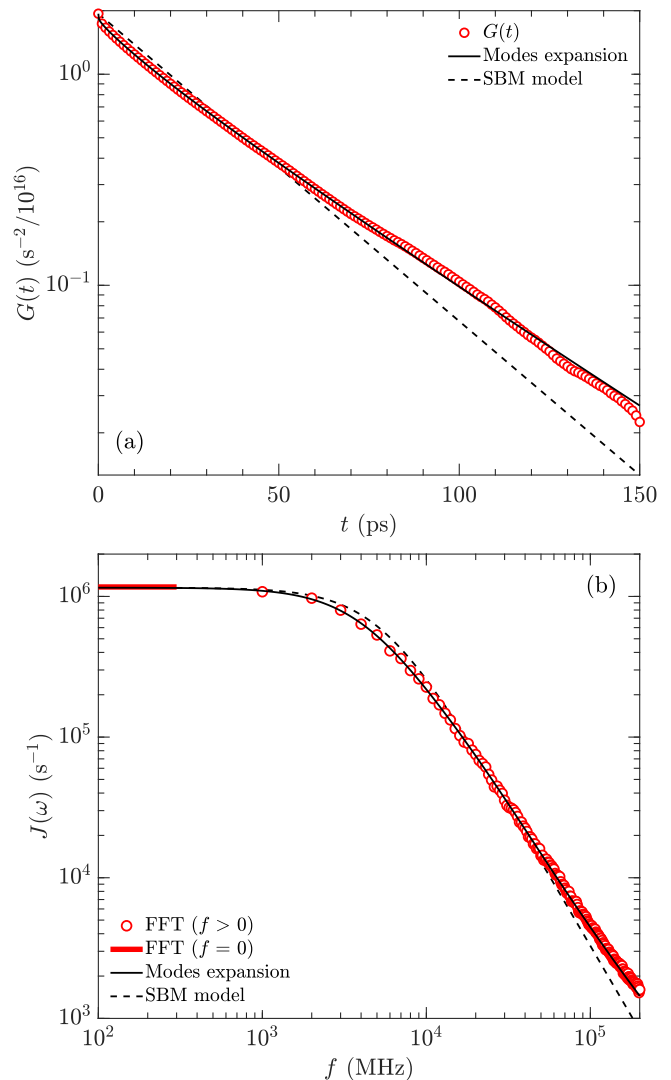


Fig. 4 (a) MD simulations of the autocorrelation function $G(t)$, where 1 in 10 data points are shown for clarity. Also shown is the modes expansion (Eq. 16) to $G(t)$, and SBM model (Eq. 25) with $\tau_R = \langle \tau \rangle = 30 \text{ ps}$. (b) Spectral density functions $J(\omega)$ from FFT (fast Fourier transform) (Eq. 8), including the $f = 0$ data point represented as a horizontal line placed at low frequency. Also shown is the modes expansion (Eq. 21), and the SBM model which tends to f^{-2} at high-frequencies.

is independent of i) reduces the second moment to:

$$\Delta\omega_i^2 = \frac{3}{5} \left(\frac{\mu_0}{4\pi} \right)^2 \hbar^2 \gamma_I^2 \gamma_S^2 S(S+1) \left\langle \frac{1}{r_i^6(t')} \right\rangle. \quad (7)$$

The next step is to take the (two-sided even) fast Fourier transform (FFT) of the $G_i(t)$ to obtain the spectral density function:

$$J_i(\omega) = 2 \int_0^\infty G_i(t) \cos(\omega t) dt. \quad (8)$$

The relaxation rates are then determined for unlike spins⁶⁸:

$$\frac{1}{T_{1i}} = J_i(\omega_0) + \frac{7}{3}J_i(\omega_e), \quad (9)$$

$$\frac{1}{T_{2i}} = \frac{2}{3}J_i(0) + \frac{1}{2}J_i(\omega_0) + \frac{13}{6}J_i(\omega_e), \quad (10)$$

assuming $\omega_e \gg \omega_0$, where $\omega_0 = \gamma B_0 = 2\pi f_0$ is the ^1H NMR resonance frequency, and $\omega_e = 658 \omega_0$ is the electron resonance frequency.

The expressions for $T_{1i,2i}$ are then summed in Eqs. 3 and 4 to compute r_1 and r_2 , respectively. We also define the following quantities summed over the $N = 1024$ ^1H nuclei:

$$G(t) = \sum_{i=1}^N G_i(t), \quad (11)$$

$$\Delta\omega^2 = \sum_{i=1}^N \Delta\omega_i^2 \quad (12)$$

$$J(\omega) = \sum_{i=1}^N J_i(\omega). \quad (13)$$

Note that the summed quantities $G(t)$, $\Delta\omega^2$, and $J(\omega)$ are independent of N (or box size L , equivalently). The $G(t)$ simulation data is plotted in Fig 4(a), while the $J(\omega)$ simulation data is plotted in Fig 4(b).

We also define the average correlation time $\langle\tau\rangle$ as the normalized integral⁶⁹:

$$\langle\tau\rangle = \frac{1}{G(0)} \int_0^\infty G(t) dt. \quad (14)$$

The low frequency (i.e. extreme narrowing) limit $r_1(0) = r_2(0) = r_{1,2}(0)$ can then be expressed as:

$$r_{1,2}(0) = \frac{1}{[H]} \frac{20}{9} \Delta\omega^2 \langle\tau\rangle. \quad (15)$$

Note how $r_{1,2}(0)$ (for unlike $\text{Gd}^{3+}\text{-}^1\text{H}$ spin pairs) is a factor 2/3 less than the equivalent expression for like $^1\text{H}\text{-}^1\text{H}$ spin pairs⁵⁰.

We assume the ‘‘fast-exchange’’ regime in the above formulation, which is discussed in more detail in Section 3.2. The fast-exchange regime can be inferred directly from measurements since r_1 increases with decreasing temperature¹⁶. Investigations are underway to extend the simulations to the slow-exchange regime.

The above analysis also assumes the electron spin is a point-dipole centered at the Gd^{3+} ion⁴. Given that the simulation agrees with measurements in the range $f_0 \simeq 5 \leftrightarrow 500$ MHz, the point-dipole approximation is considered valid in the present case for ^1H ¹⁰.

2.5 Expansion of $G(t)$ in terms of molecular modes

The FFT result for $J(\omega)$ in Fig. 4(b) is sparse. Besides the $f = 0$ data point, the lowest frequency FFT data point is given by the resolution $\Delta f = 1/2t_{max} = 10^3$ MHz, where $t_{max} = 500$ ps is the longest lag time in $G(t)$.

As an alternative to zero-padding the FFT, we see to model $G(t)$ in terms of molecular modes. To this end, we expand $G(t)$ as

$$G(t) = \int_0^\infty P(\tau) \exp\left(-\frac{t}{\tau}\right) d\tau, \quad (16)$$

where $P(\tau)$ is the underlying distribution in molecular correlation times, τ . We solve this Fredholm integral equation of the first kind to recover the $P(\tau)$ distribution. Since $G(t)$ is available only at discrete time intervals, the inversion is an ill-posed problem. We address this by using Tikhonov regularization^{52,73}, with the vector \mathbf{P} being one for which

$$\mathbf{P} = \arg \min_{\mathbf{P} \geq 0} \|\mathbf{G} - \mathbf{K}\mathbf{P}\|^2 + \alpha \|\mathbf{P}\|^2 \quad (17)$$

is a minimum. Here \mathbf{G} is the column vector representation of the autocorrelation function $G(t)$, \mathbf{P} is the column vector representation of the distribution function $P(\tau)$, α is the regularization parameter, and K is the kernel matrix:

$$K = K_{ij} = \exp\left(-\frac{t_i}{\tau_j}\right). \quad (18)$$

The results for $P(\tau)$ are shown in Fig. 5, from which the following are determined:

$$\langle\tau\rangle = \frac{1}{G(0)} \int_0^\infty P(\tau) \tau d\tau, \quad (19)$$

$$G(0) = \int_0^\infty P(\tau) d\tau = \frac{1}{3} \Delta\omega^2. \quad (20)$$

The spectral density $J(\omega)$ is then determined from the Fourier transform (Eq. 8) of $G(t)$ (Eq. 16):

$$J(\omega) = \int_0^\infty \frac{2\tau}{1 + (\omega\tau)^2} P(\tau) d\tau, \quad (21)$$

from which $T_{1,2}$ at any desired f_0 can be determined (Eqs. 9 and 10). More in-depth discussions of the above procedure, loosely termed as ‘‘inverse Laplace transform’’, can be found in Refs.^{53–56,74,75} and the supplementary material in Refs.^{52,73}. We hasten to add that inverting Eq. 16 to recover P is formally not a Laplace inversion⁷⁶, but this terminology is common in the literature. Possible alternatives to the above formulation are also discussed in Ref.⁵³.

The $P(\tau)$ is binned from $\tau_{min} = 0.05$ ps to $\tau_{max} = 500$ ps using 200 logarithmically spaced bins. In the present case of low-viscosity fluids ($\eta \simeq 1$ cP), the choice of τ_{max} does not impact $J(\omega)$, and is therefore *not* a free parameter in the analysis in terms of molecular modes. The constant ‘‘div’’ in Fig. 5 is a ‘‘division’’ on a log-scale. More specifically, $\text{div} = \log_{10}(\tau_{i+1}) - \log_{10}(\tau_i)$ is independent of the bin index i , and ensures unit area when $P(\tau)$ is of unit height and a decade wide⁷³.

As shown in Fig. 4(a), the residual between the $G(t)$ data and the fit using molecular modes is not dominated by Gaussian noise. As such, the regularization parameter is fixed to $\alpha = 10^{-1}$ in accordance with previous studies^{52–56}. As shown in Fig. 4(b), we find that $\alpha = 10^{-1}$ gives excellent agreement with the parameter-free $J(\omega)$ from FFT, which validates the anal-

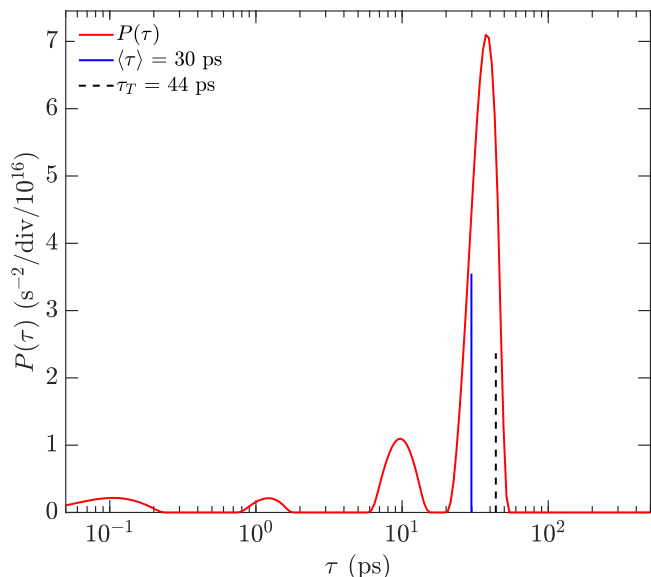


Fig. 5 Probability density function $P(\tau)$ obtained from the expansion of molecular modes (Eq. 16) of $G(t)$. The average correlation time $\langle\tau\rangle$ (Table 1) and predicted translational correlation time τ_T (Table 3) are shown.

ysis in terms of molecular modes. The results in Fig. 4(b) further emphasize the following advantages: (1) the expansion (Eq. 16) filters out the noise while still honoring the FFT data (including the $f = 0$ data point), (2) Eq. 21 provides $J(\omega)$ for any desired f value, and (3) the expansion in terms of molecular modes leads to physical insight into the distribution $P(\tau)$ of molecular correlation times τ .

2.6 Diffusion

An independent computation of translational diffusion D_T was performed from MD simulations. We calculate the mean square displacement $\langle\Delta r^2\rangle$ of the water oxygen and Gd^{3+} ion as a function of the diffusion evolution time t (< 10 ps). For bulk water (i.e., without Gd^{3+}), the data is taken from Ref. 50, where we average over a sample of 50 molecules to ensure adequate statistical convergence. For water in Gd^{3+} -aqua, we sampled all the water molecules to capture adequately the effects of exchanging with the inner shell.

As shown in Fig. 6, at long-times (t) the slope of the linear diffusive regime gives the translational self-diffusion coefficient D_{sim} according to Einstein's relation:

$$D_{sim} = \frac{1}{6} \frac{\delta\langle\Delta r^2\rangle}{\delta t} \quad (22)$$

where D_{sim} is the diffusion coefficient obtained in the simulation using periodic boundary conditions in a cubic cell of length L . In the linear regression procedure, the early ballistic regime and part of the linear regime is excluded to obtain a robust estimate of D_{sim} .

Following Yeh and Hummer⁷⁷ (see also Dünweg and Kremer⁷⁸), we obtain the diffusion coefficient for an infinite system

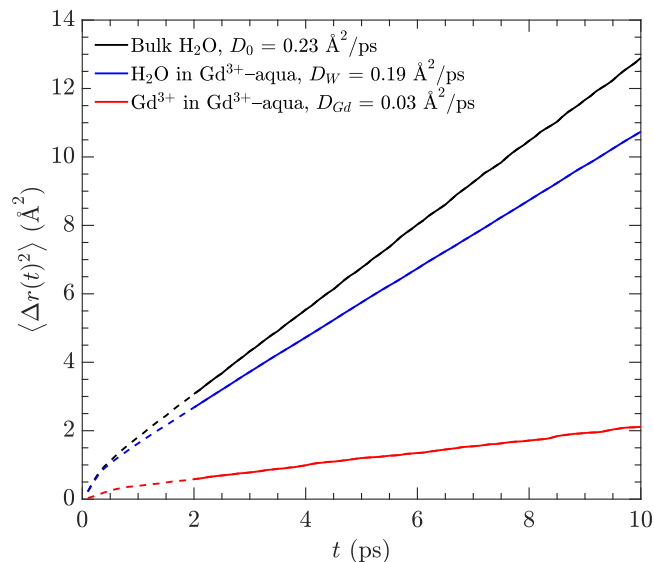


Fig. 6 MD simulations of mean-square displacement $\langle\Delta r^2\rangle$ versus time t for bulk water (i.e., without Gd^{3+}), water in Gd^{3+} -aqua, and Gd^{3+} in Gd^{3+} -aqua. Solid lines show fitting region used to obtain translational diffusion coefficient D_{sim} from Eq. 22 for $t > 2$ ps, and dashed lines show early time regime not used in the fit. Legend indicates D_T values which include the correction term (Eq. 23).

D_T from D_{sim} using

$$D_T = D_{sim} + \frac{k_B T \xi}{6\pi\eta L} \quad (23)$$

where η is the shear viscosity and $\xi = 2.837297^{77}$ is the same quantity that arises in the calculation of the Madelung constant in electrostatics. (In the electrostatic analog of the hydrodynamic problem, ξ/L is the potential at the charge site in a Wigner lattice.) For the system sizes considered in this study, $L \simeq 25$ Å, the correction factor constituted $\simeq 13\%$ of D_0 , and $\simeq 16\%$ of D_W . The correction factor was not applied to D_{Gd} .

2.7 Measurements

We prepared a Gd^{3+} -aqua solution in de-ionized water at $[\text{Gd}] = 0.3$ mM and measured $T_{1,meas}$ at a controlled temperature of 25°C , using static fields at $f_0 = 2.3$ MHz with an Oxford Instruments GeoSpec2, at $f_0 = 20$ MHz with a Bruker Minispec, and at $f_0 = 500$ MHz with a Bruker 500 MHz Spectrometer. The measured relaxivity r_1 was determined as such:

$$r_1 = \frac{1}{[\text{Gd}]} \left(\frac{1}{T_{1,meas}} - \frac{1}{T_{1,bulk}} \right). \quad (24)$$

where $T_{1,bulk} = 3.13$ s was found for bulk water (not de-oxygenated⁷⁹) at 2.3 MHz and 500 MHz. Field cycling r_1 data at $[\text{Gd}] = 1$ mM and 25°C were taken from Luchinat *et al.*³⁴ (supplementary material) using a Stellar SpinMaster 1T. The field cycling results agreed with our measurements at $f_0 = 2.3$ MHz and 20 MHz (within $\simeq 5\%$), while our $f_0 = 500$ MHz significantly extends the frequency range of the measurements.

3 Results and discussions

In this section we compare the simulated relaxivity r_1 with measurements. The simulated relaxivity is then discussed in the context of the Solomon-Bloembergen-Morgan (SBM) model, and Hwang-Freed (HF) model. The zero-field electron-spin relaxation time is then determined from r_1 at low frequencies.

3.1 Comparison with measurements

The results of simulated relaxivity r_1 (Eq. 3) are shown in Fig. 7, alongside corresponding measurements of Gd^{3+} -aqua solution at 25°C using field cycling by Luchinat *et al.*³⁴ (supplementary material), and static fields from this work. A cross-plot of simulated versus measured r_1 results are also shown in Fig. 8. The simulation is within $\approx 8\%$ of measurements in the range $f_0 \approx 5 \leftrightarrow 500$ MHz. Given that there are no adjustable parameters in the interpretation of the simulations, this agreement validates our simulations at high frequencies. We note that a similar degree of agreement (within $\approx 7\%$) was found in previous studies of liquid alkanes and water⁵⁰.

For convenience, Table 1 lists the coordination number q (Fig. 1), the residence time τ_m (Fig. 3), average correlation time $\langle\tau\rangle$ (Eq. 19), and the square-root of the second moment (i.e. strength) $\Delta\omega$ (Eq. 20). Note that these quantities are model independent. Also listed is the the zero-field electron-spin relaxation time T_{e0} (Eq. 32), which only assumes that the correlation times $P(\tau)$ are uncorrelated with T_{e0} .

q	τ_m (ns)	$\langle\tau\rangle$ (ps)	$\Delta\omega/2\pi$ (MHz)	T_{e0} (ps)
8.5	1 \leftrightarrow 2	30	38.4	180

Table 1 Analysis of the simulation results including; coordination number q (Fig. 1), residence time τ_m (Fig. 3), mean correlation time $\langle\tau\rangle$ (Eq. 19), and square-root of second moment $\Delta\omega$ (Eq. 20), all of which are model independent. Right: zero-field electron-spin relaxation time T_{e0} (Eq. 32).

3.2 SBM inner-sphere model

The SBM inner-sphere model assumes a rigid Gd^{3+} - ^1H pair undergoing rotational diffusion, leading to the following mono-exponential decay in the autocorrelation function:

$$G_{SBM}(t) = G_{SBM}(0) \exp\left(-\frac{t}{\tau_R}\right). \quad (25)$$

This functional form is identical to the BPP model⁴⁷ which is based on the Debye theory, where the rotational-diffusion correlation time τ_R is defined as the average time it takes the rigid pair to rotate by 1 radian. $G_{SBM}(t)$ is plotted in Fig. 4(a) assuming $\tau_R = \langle\tau\rangle = 30$ ps.

As shown in Fig. 4(a), the mono-exponential decay in $G_{SBM}(t)$ is not consistent with the multi-exponential (i.e., stretched) decay in $G(t)$. Equivalently, $J(\omega)$ in Fig. 4(b) does not follow the f^{-2} power-law behavior at large f . This is expected since the simulations implicitly include both inner-sphere and outer-sphere (see

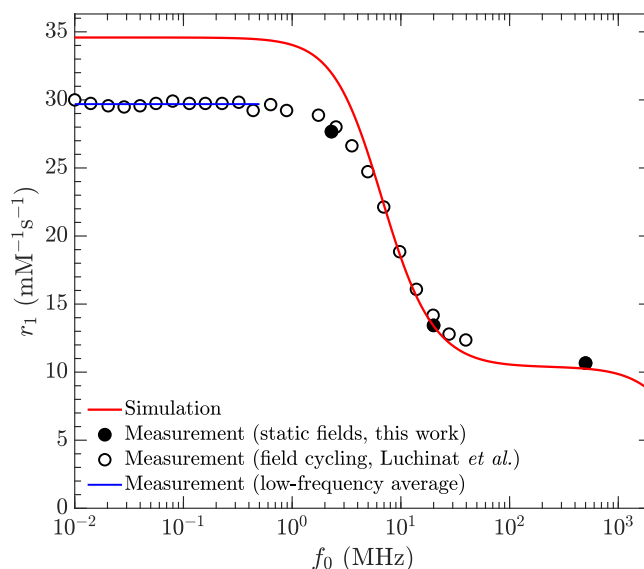


Fig. 7 Simulated ^1H NMR relaxivity r_1 of Gd^{3+} -aqua solution at 25°C, compared with static-field measurements (this work) and field-cycling measurements (Luchinat *et al.*³⁴, supplementary material). Also shown is the average of the low-frequency ($f_0 < 0.5$ MHz) measurements.

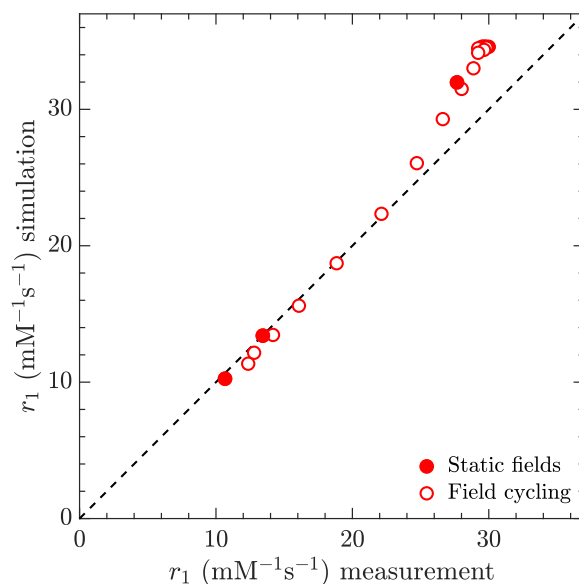


Fig. 8 Cross-plot of measured r_1 (including static-field and field-cycling measurements) versus simulations taken from Fig. 7, all at 25°C. Dashed line is the 1-1 unity line.

below) contributions. Currently the simulations do not separate inner-sphere from outer-sphere contributions, therefore the simulations do not clarify the origin of the multi-exponential decay in $G(t)$.

It is also possible that the inner-sphere $G(t)$ itself has a multi-exponential decay. The functional form of $G_{SBM}(t)$ is based on the Debye theory, which was previously shown to be inaccurate when used in the BPP model for liquid alkanes and water⁵⁰. It would therefore not be surprising if the inner-sphere $G(t)$ was also multi-exponential given the more complex rotational dynamics of

τ_R	r_{in}	$\Delta\omega_{in}/2\pi$	$T_{1in}(0)$	r_H
(ps)	(Å)	(MHz)	(μ s)	(Å)
30	2.97	9.3	4.4	3.06

Table 2 Approximate inner-sphere quantities (assuming inner-sphere relaxation dominates) including rotation correlation time $\tau_R (= \langle \tau \rangle)$, Table 1), Gd³⁺-¹H distance r_{in} (Eq. 26), square-root of second moment $\Delta\omega_{in}$ (Eq. 27), and relaxation time $T_{1in}(0)$ at $f_0 = 0$ (Eq. 28); (right) Gd-H distance r_H for the inner-sphere taken from $g_{Gd-H}(r)$ in Fig. 1.

Gd³⁺-aqua compared to bulk water. Previous reports have shown that the inner-sphere $G(t)$ for Gd³⁺-aqua is consistent with a mono-exponential decay³³, however those simulations were not validated against measurements.

Assuming that inner-sphere relaxation dominates, and therefore that the multi-exponential decay in $G(t)$ is due to inner-sphere dynamics alone, the correlation time $\langle \tau \rangle \simeq 30$ ps is consistent with published values from the SBM inner-sphere model, where a range of $\tau_R \simeq 23 \leftrightarrow 45$ ps is reported^{16,18,22,23,25,33,34}. Note that $\langle \tau \rangle \simeq 30$ ps is a factor $\simeq 10$ larger than that of bulk water ($\tau_R \simeq 2.7$ ps⁵⁰), which is expected given the hindered rotational motion of the Gd³⁺-aqua complex.

Continuing with the assumption that inner-sphere relaxation dominates, one can approximate the following inner-sphere quantities:

$$\frac{1}{r_{in}^6} \simeq \frac{1}{2q} \sum_{i=1}^N \left\langle \frac{1}{r_i^6(t')} \right\rangle \quad (26)$$

$$\Delta\omega_{in}^2 \simeq \frac{1}{2q} \sum_{i=1}^N \Delta\omega_i^2 \quad (27)$$

$$\frac{1}{T_{1in}} \simeq \frac{1}{2q} \sum_{i=1}^N \frac{1}{T_{1i}} \quad (28)$$

The expressions are averaged over the $2q$ ¹H nuclei in the inner sphere, where $q = 8.5$ (Table 1). Note again that these equations neglect the outer-sphere contribution, implying that $\Delta\omega_{in}^2$ is an upper bound, while r_{in} and $T_{1in}(0)$ are lower bounds.

According to Table 2, the resulting $r_{in} \simeq 2.97$ Å is $\simeq 3\%$ lower than $r_H \simeq 3.06$ Å from $g_{Gd-H}(r)$ in Fig. 1; this is expected given that r_{in} is a lower bound. Both r_{in} and r_H are consistent with published values from the inner-sphere SBM model, where a range of $r \simeq 3.0 \leftrightarrow 3.2$ Å is reported^{16,18,22,23,25,33,34}.

The product $\Delta\omega_{in} \tau_R \simeq 0.002$ indicates that the Redfield-Bloch-Wagners condition ($\Delta\omega \langle \tau \rangle \ll 1$) is satisfied⁶⁷⁻⁶⁹, which justifies the relaxivity analysis used here. The fast-exchange regime¹¹ can also be verified by noting that $T_{1in}(0) \simeq 4.4$ μ s at $f_0 = 0$ is three orders of magnitude larger than $\tau_m \simeq 1$ ns, i.e. $(T_{1in} + \tau_m) \simeq T_{1in}$ can be assumed.

3.3 HF outer-sphere model

We now discuss the outer-sphere contribution to relaxivity, although it is generally believed (though not proven) to be smaller than inner-sphere relaxivity^{16,19,24}. The outer-sphere contribu-

tion is expected to follow the Hwang-Freed (HF) model for the relative translational diffusion between Gd³⁺ and H₂O assuming two force-free hard-spheres⁶:

$$G_{HF}(t) = G_{HF}(0) \frac{54}{\pi} \int_0^\infty \frac{x^2}{81 + 9x^2 - 2x^4 + x^6} \times \exp\left(-x^2 \frac{t}{\tau_D}\right) dx. \quad (29)$$

The translational-diffusion correlation time τ_D is defined as the average time it takes the molecule to diffuse by one hard-core diameter d_O . $G_{HF}(t)$ is a multi-exponential decay by nature, and therefore one expects the total $G(t)$ to also be multi-exponential, the extent of which depends on the relative contributions of outer-sphere to inner-sphere.

The correlation time τ_D can be predicted as such:

$$\tau_D = \frac{d_O^2}{D_W + D_{Gd}} = \frac{9}{4} \tau_T, \quad (30)$$

where the simulated diffusion coefficients of H₂O (D_W) and Gd³⁺ (D_{Gd}) in Gd³⁺-aqua are taken from Fig. 6, the results of which are listed in Table 3. The hard-core diameter d_O is taken from the local maximum at $r \simeq 4.6$ Å in the pair-correlation function $g_{Gd-O}(r)$ in Fig. 1 (which is attributed to outer-sphere water). Note that the resulting $\tau_D \simeq 99$ ps is a factor $\simeq 10$ larger than that of bulk water ($\tau_D \simeq 9.0$ ps⁵⁰), which is expected given the larger hard-core distance $d_O \simeq 4.6$ Å than bulk water ($d_O \simeq 2.0$ Å⁵⁰).

D_W	D_{Gd}	d_O	τ_D	τ_T
(Å ² /ps)	(Å ² /ps)	(Å)	(ps)	(ps)
0.19	0.03	4.6	99	44

Table 3 Diffusion coefficients of H₂O (D_W) and Gd³⁺ (D_{Gd}) in Gd³⁺-aqua, distance of closest approach (d_O) between Gd³⁺ and outer-sphere H₂O according to $g_{Gd-O}(r)$ (Fig. 1), and, resulting translational-diffusion correlation time $\tau_D (= 9/4 \tau_T)$ from Eq. 30.

The value $\tau_D \simeq 99$ ps is compared to the distribution of molecular modes $P(\tau)$ in Fig. 5. More specifically, the translational correlation time $\tau_T \simeq 44$ ps is plotted in Fig. 5, where the relation $\tau_D = 9/4 \tau_T$ and the origin of the factor $9/4$ is explained in^{52,69}. τ_T lies within the largest mode in $P(\tau)$ (with a peak at $\tau \simeq 36$ ps), indicating that the outer-sphere may contribute to relaxivity. Further investigations are underway to separate inner-sphere from outer-sphere contributions in the simulations, without assuming any models.

The largest mode in $P(\tau)$ is, however, most likely associated with the rotational motion of the Gd³⁺-H₂O vector. $P(\tau)$ has other modes too, including a smaller mode at short $\tau \simeq 10^{-1}$ ps, which is a result of the sharp drop in $G(t)$ over the initial $t \simeq 0.2$ ps (Fig. 4(a)). This molecular mode is also present for intramolecular relaxation in liquid alkanes and water, while it is absent for intermolecular relaxation. In the case of alkanes, the ubiquitous intramolecular mode at $\tau \simeq 10^{-1}$ ps is attributed to the fast spin-

ning methyl end-groups^{52,80}. Investigations are underway to better understand the origin of this mode in Gd^{3+} -aqua, which can perhaps be explained using a two rotational-diffusion model such as found in bulk water⁸¹. The origin of other modes in $P(\tau)$ at $\tau \simeq 10^0$ ps and $\simeq 10^1$ ps are also being investigated.

Finally, we note that the r_1 dispersion in Fig. 7 results in a mild increase in the ratio $T_1/T_2 = r_2/r_1 \simeq 7/6$ above $f_0 \gtrsim 10$ MHz, until $f_0 \gtrsim 6$ GHz where T_1/T_2 increases further. Combining Eqs. 9 and 10 with $J(\omega_e) = 0$ (i.e., slow-motion regime) and $J(\omega_0) = J(0)$ (i.e., fast-motion regime) accounts for the factor $T_1/T_2 = 7/6$ within the frequency range $f_0 \simeq 10$ MHz \leftrightarrow 6 GHz. The ratio $T_1/T_2 = 7/6$ was also used to explain water-saturated sandstones⁴⁰.

3.4 Electron-spin relaxation

At low-frequencies ($f_0 \lesssim 0.5$ MHz), the difference between r_1 measurements ($r_1(0) \simeq 29.7 \text{ mM}^{-1}\text{s}^{-1}$) and simulation ($r_1(0) \simeq 34.6 \text{ mM}^{-1}\text{s}^{-1}$) can be used to predict the zero-field electron-spin relaxation time $T_{e0} = T_{1e}(0) = T_{2e}(0)$ into account. Assuming that the correlation times $P(\tau)$ are uncorrelated with the electron-spin relaxation times, the following expression results³:

$$r'_{1,2}(0) = \frac{1}{[H]} \frac{20}{9} \Delta\omega^2 \langle \tau' \rangle, \quad (31)$$

$$\frac{1}{\langle \tau' \rangle} = \frac{1}{\langle \tau \rangle} + \frac{1}{T_{e0}}. \quad (32)$$

This is equivalent to introducing an exponential decay term $\exp(-t/T_{e0})$ inside the FFT integral of Eq. 8. The fitted value of $T_{e0} \simeq 180$ ps is determined by matching $r'_1(0)$ to the average low-frequency ($f_0 \lesssim 0.5$ MHz) measurement (Fig. 7). The resulting $T_{e0} \simeq 180$ ps (Table 1) is consistent with the published range of $T_{e0} \simeq 96 \leftrightarrow 160$ ps^{16,18,22,23,25,33,34}. This technique presents a novel way to predict T_{e0} , without assuming any relaxation models. Investigations are underway to incorporate $T_{1e}(\omega_e)$ and $T_{2e}(\omega_e)$ dispersion^{4,25,28,33} for predicting r_1 at low frequencies.

4 Conclusions

Atomistic MD simulations of ^1H NMR relaxivity r_1 for water in Gd^{3+} -aqua complex at 25°C show good agreement (within $\simeq 8\%$) with measurements in the range $f_0 \simeq 5 \leftrightarrow 500$ MHz, without any adjustable parameters in the interpretation of the simulations, and without any relaxation models. This level of agreement validates the simulation techniques and analysis of Gd^{3+} - ^1H dipole-dipole relaxation for unlike spins.

The distribution of continuous occupancy times of the inner sphere suggests residence times between $\tau_m \simeq 1 \leftrightarrow 2$ ns for a complete rejuvenation of the inner-sphere waters of Gd^{3+} . Further, the average coordination number is $q \simeq 8.5$. These observations from simulation are consistent with previously reported interpretation of experiments using the SBM model.

The simulated autocorrelation function $G(t)$ shows a multi-exponential decay, with an average correlation time of $\langle \tau \rangle \simeq 30$ ps. The multi-exponential nature of $G(t)$ is expected given that the simulation implicitly includes both inner-sphere and outer-sphere contributions. The results are analyzed assuming that the

inner-sphere relaxation dominates, yielding approximations for the average Gd^{3+} - ^1H separation $r_{in} \simeq 2.97 \text{ \AA}$ and rotational correlation time $\tau_R = \langle \tau \rangle \simeq 30$ ps, both of which are consistent with previously published values which use the Solomon-Bloembergen-Morgan (SBM) model. The local maximum in $g_{\text{Gd-H}}(r)$ for inner-sphere water predicts $r_H \simeq 3.06 \text{ \AA}$ for the average Gd^{3+} - ^1H separation, which is also consistent with previously published values.

A distance of closest approach (i.e. hard-core diameter) for Gd^{3+} - H_2O of $d_O \simeq 4.64 \text{ \AA}$ is determined from the local maximum in $g_{\text{Gd-O}}(r)$ (attribute to outer-sphere water), which together with the simulated diffusion coefficients of Gd^{3+} and H_2O are used to estimate the translational-diffusion correlation time $\tau_D = 9/4 \tau_T \simeq 99$ ps in the Hwang-Freed (HF) outer-sphere model. Comparing τ_T to the distribution in molecular modes $P(\tau)$ (determined from the modes expansion of $G(t)$) indicates that the outer-sphere may contribute to relaxivity.

Below $f_0 \lesssim 5$ MHz the simulation overestimates r_1 compared to measurements, which is used to estimate the zero-field electron-spin relaxation time T_{e0} . The resulting fitted value $T_{e0} \simeq 180$ ps is consistent with the published range of values. This technique presents a novel way to predict T_{e0} , without assuming any relaxation models.

The excellent agreement of r_1 at high frequencies ($f_0 \gtrsim 5$ MHz) for Gd^{3+} -aqua complexes provides a pathway to explore Gd^{3+} chelates with cyclic, acyclic, and protein-bound metals ligands. Understanding the roles of relaxation induced by these paramagnetic chelated complexes is crucial given their use as clinical MRI contrast agents, where $f_0 \simeq 64$ MHz (1.5 T) is the typical MRI operating frequency. Thus, for future work, we plan to study Gd^{3+} - ^1H NMR relaxation of clinical contrast agents such as $[\text{Gd}(\text{DOTA})(\text{H}_2\text{O})]^-$ and $[\text{Gd}(\text{DTPA})(\text{H}_2\text{O})]^{2-}$ in aqua.

Other possibilities for future work include (1) simulations in the slow-exchange regime (as opposed to fast-exchange regime), (2) separation of inner-sphere from outer-sphere contributions, (3) interpretation of the individual molecular-modes in $P(\tau)$, (4) predicting electron-spin relaxation dispersion (i.e., not just the zero-field value T_{e0}), and (5) simulating dipole-dipole cross-correlation (as opposed to autocorrelation), which for anisotropic rotation can result in multi-exponential T_1 and T_2 relaxation.

Conflicts of interest

There are no conflicts to declare.

Acknowledgements

We thank Vinegar Technologies LLC, Chevron Energy Technology Company, and the Rice University Consortium on Processes in Porous Media for financial support. We gratefully acknowledge the National Energy Research Scientific Computing Center, which is supported by the Office of Science of the U.S. Department of Energy (No. DE-AC02-05CH11231) and the Texas Advanced Computing Center (TACC) at The University of Texas at Austin for high-performance computer time and support.

Notes and references

- 1 I. Solomon, *Phys. Rev.*, 1955, **99**, 559–565.
- 2 N. Bloembergen, *J. Chem. Phys.*, 1957, **27**, 572–573.

- 3 N. Bloembergen and L. O. Morgan, *J. Chem. Phys.*, 1961, **34**, 842–850.
- 4 J. Kowalewski, L. Nordenskiöld, N. Benetis and P.-O. Westlund, *Prog. Nucl. Magn. Reson. Spect.*, 1985, **17**, 141–185.
- 5 H. C. Torrey, *Phys. Rev.*, 1953, **92**, 962–969.
- 6 L.-P. Hwang and J. H. Freed, *J. Chem. Phys.*, 1975, **63**, 4017–4025.
- 7 L. O. Morgan and A. W. Nolle, *J. Chem. Phys.*, 1959, **31**, 365–368.
- 8 R. A. Bernheim, T. H. Brown, H. S. Gutowsky and D. E. Woessner, *J. Chem. Phys.*, 1959, **30**, 905–956.
- 9 P. H. Fries, G. Ferrante, E. Belorizky and S. Rast, *J. Chem. Phys.*, 2003, **119**, 8636.
- 10 L. Helm, *Prog. Nucl. Magn. Reson. Spect.*, 2006, **49**, 45–64.
- 11 J. Korrinda, D. O. Seevers and H. C. Torrey, *Phys. Rev.*, 1962, **127**, 1143–1150.
- 12 P.-O. Westlund, *Dynamics of Solutions and Fluid Mixtures by NMR*, John Wiley & Son, Chichester, 1995, p. 174–229.
- 13 S.-W. Hong, Y. Chang, M.-J. Hwang, I.-S. Rhee and D.-S. Kang, *J. Kor. Soc. Mag. Res. Med.*, 2000, **4**, 27–33.
- 14 J. Kowalewski and L. Mäler, *Nuclear Spin Relaxation in Liquids: Theory, Experiments, and Applications*, Taylor & Francis Group, 2006.
- 15 E. Belorizky, P. H. Fries, L. Helm, J. Kowalewski, D. Kruk, R. R. Sharp and P.-O. Westlund, *J. Chem. Phys.*, 2008, **128**, 052315.
- 16 S. H. Koenig and M. Epstein, *J. Chem. Phys.*, 1975, **63**, 2279.
- 17 R. V. Southwood-Jones, W. L. Earl, K. E. Newman and A. E. Merbach, *J. Chem. Phys.*, 1980, **73**, 5909.
- 18 L. Banci, I. Bertini and C. Luchinat, *Inorgan. Chimica Acta*, 1985, **100**, 173–181.
- 19 R. B. Lauffer, *Chem. Rev.*, 1987, **87**, 901–927.
- 20 S. H. Koenig and R. D. B. III, *Prog. Nucl. Magn. Reson. Spect.*, 1990, **22**, 487–567.
- 21 K. Micskei, D. H. Powell, L. Helm, E. Brücher and A. E. Merbach, *Magn. Res. Chem.*, 1993, **31**, 1011–1020.
- 22 E. Strandberg and P.-O. Westlund, *J. Magn. Reson.*, 1996, **25**, 261–266.
- 23 D. H. Powell, O. M. N. Dhubhghaill, D. Pubanz, L. Helm, Y. S. Lebedev, W. Schlaepfer and A. E. Merbach, *J. Amer. Chem. Soc.*, 1996, **118**, 9333–9346.
- 24 P. Caravan, J. J. Ellison, T. J. McMurry and R. B. Lauffer, *Chem. Rev.*, 1999, **99**, 2293–2352.
- 25 S. Rast, P. H. Fries, E. Belorizky, A. Borel, L. Helm and A. E. Merbach, *J. Chem. Phys.*, 2001, **115**, 7554.
- 26 A. E. Merbach and Éva Tóth, *The Chemistry of Contrast Agents in Medical Magnetic Resonance Imaging*, John Wiley & Sons, Chichester, UK, 2011.
- 27 I. Bertini, C. Luchinat and G. Parigi, *Solution NMR of Paramagnetic Molecules; Applications to Metallobiomolecules and Models*, Elsevier, 2001.
- 28 A. Borel, F. Yerly, L. Helm and A. E. Merbach, *J. Amer. Chem. Soc.*, 2002, **124**, 2042–2048.
- 29 X. Zhou, P. Caravan, R. B. Clarkson and P.-O. Westlund, *J. Magn. Reson.*, 2004, **167**, 147–160.
- 30 X. Zhou and P.-O. Westlund, *Spectrochim. Acta A*, 2005, **62**, 76–82.
- 31 O. V. Yazyev and L. Helm, *J. Chem. Phys.*, 2007, **127**, 084506.
- 32 O. V. Yazyev and L. Helm, *Eur. J. Inorg. Chem.*, 2008, 201–211.
- 33 M. Lindgren, A. Laaksonen and P.-O. Westlund, *Phys. Chem. Chem. Phys.*, 2009, **11**, 10368–10376.
- 34 C. Luchinat, G. Parigi and E. Ravera, *J. Biomol. NMR*, 2014, **58**, 239–249.
- 35 S. Aime, M. Botta, D. Esteban-Gómez and C. Platas-Iglesias, *Mol. Phys.*, 2019, **117**, 898–909.
- 36 M. Fragai, E. Ravera, F. Tedoldi, C. Luchinat and G. Parigi, *ChemPhysChem*, 2019, **20**, 2204–2209.
- 37 H. Li and T. J. Meade, *J. Amer. Chem. Soc.*, 2019, **141**, 17025–17041.
- 38 J. Wahsner, E. M. Gale, A. Rodríguez-Rodríguez and P. Caravan, *Chem. Rev.*, 2019, **119**, 957–1057.
- 39 R. L. Kleinberg, W. E. Kenyon and P. P. Mitra, *J. Magn. Reson.*, 1994, **108**, 206–214.
- 40 I. Foley, S. A. Farooqui and R. L. Kleinberg, *J. Magn. Reson.*, 1996, **123**, 95–104.
- 41 C. Straley, *Soc. Core Analysts*, 2002, **SCA2002**, 27.
- 42 G. Q. Zhang, G. J. Hirasaki and W. V. House, *Petrophysics*, 2003, **44**, 422–434.
- 43 J.-P. Korb, G. Freiman, B. Nicot and P. Ligneul, *Phys. Rev. E*, 2009, **80**, 061601.
- 44 J. Mitchell, L. F. Gladden, T. C. Chandrasekera and E. J. Fordham, *Prog. Nucl. Magn. Reson. Spect.*, 2014, **76**, 1–60.
- 45 D. A. Faux, S. H. P. Cachia, P. J. McDonald, J. S. Bhatt, N. C. Howlett and S. V. Churakov, *Phys. Rev. E*, 2015, **91**, 032311.
- 46 M. Saidian and M. Prasad, *Fuel*, 2015, **161**, 197–206.
- 47 N. Bloembergen, E. M. Purcell and R. V. Pound, *Phys. Rev.*, 1948, **73**, 679–712.
- 48 G. Lipari and A. Szabo, *J. Amer. Chem. Soc.*, 1982, **104**, 4546–4559.
- 49 G. Lipari and A. Szabo, *J. Amer. Chem. Soc.*, 1982, **104**, 4559–4570.
- 50 P. M. Singer, D. Asthagiri, W. G. Chapman and G. J. Hirasaki, *J. Magn. Reson.*, 2017, **277**, 15–24.
- 51 D. Asthagiri, P. M. Singer, A. Valiya Parambathu, Z. Chen, G. J. Hirasaki and W. G. Chapman, *SEG/AAPG/EAGE/SPE Research and Development Petroleum Conference and Exhibition*, 2018, 101–102.
- 52 P. M. Singer, D. Asthagiri, Z. Chen, A. Valiya Parambathu, G. J. Hirasaki and W. G. Chapman, *J. Chem. Phys.*, 2018, **148**, 164507.
- 53 D. Asthagiri, W. G. Chapman, G. J. Hirasaki and P. M. Singer, *J. Phys. Chem. B*, 2020, **124**, 10802–10810.
- 54 P. M. Singer, D. Asthagiri, W. G. Chapman and G. J. Hirasaki, *J. Chem. Phys.*, 2018, **148**, 204504.
- 55 P. M. Singer, A. Valiya Parambathu, X. Wang, D. Asthagiri, W. G. Chapman, G. J. Hirasaki and M. Fleury, *J. Phys. Chem. B*, 2020, **124**, 4222–4233.
- 56 A. Valiya Parambathu, P. M. Singer, G. J. Hirasaki, W. G. Chap-

- man and D. Asthagiri, *J. Phys. Chem. B*, 2020, **124**, 3801–3810.
- 57 P. Ren and J. W. Ponder, *J. Phys. Chem. B*, 2003, **107**, 5933–5947.
- 58 C. Clavaguéra, F. Calvo and J.-P. Dognon, *J. Chem. Phys.*, 2006, **124**, 074505.
- 59 D. Asthagiri, L. R. Pratt, M. E. Paulaitis and S. B. Rempe, *J. Amer. Chem. Soc.*, 2004, **126**, 1285–1289.
- 60 P. Eastman, J. Swails, J. D. Chodera, R. T. McGibbon, Y. Zhao, K. A. Beauchamp, L. P. Wang, A. C. Simmonett, M. P. Harrigan, C. D. Stern, R. P. Wiewiara, B. R. Brooks and V. S. Pande, *PLOS Comp. Bio.*, 2017, **13**, e1005659.
- 61 S. Nosé, *Mol. Phys.*, 1984, **52**, 255–268.
- 62 W. G. Hoover, *Phys. Rev. A*, 1985, **31**, 1695–1697.
- 63 Z. Zhang, X. Liu, K. Yan, M. E. Tuckerman and J. Liu, *J. Phys. Chem. A*, 2019, **123**, 6056–6079.
- 64 E. J. Maginn, R. A. Messerly, D. J. Carlson, D. R. Roe and J. R. Elliott, *Living J. Comp. Mol. Sc.*, 2018, **1**, 1–20.
- 65 D. H. Powell, A. E. Merbach, G. González, E. Brücher, K. Micskei, M. F. Ottaviani, K. Köhler, A. V. Zelewsky, O. Y. Grinberg and Y. S. Lebedev, *Helv. Chim. Acta*, 1993, **76**, 2129–2146.
- 66 L. Helm and A. E. Merbach, *Coord. Chem. Rev.*, 1999, **187**, 151–181.
- 67 A. Abragam, *Principles of Nuclear Magnetism*, Oxford University Press, International Series of Monographs on Physics, 1961.
- 68 J. McConnell, *The Theory of Nuclear Magnetic Relaxation in Liquids*, Cambridge University Press, 1987.
- 69 B. Cowan, *Nuclear Magnetic Resonance and Relaxation*, Cambridge University Press, 1997.
- 70 R. Kimmich, *NMR Tomography, Diffusometry and Relaxometry*, Springer-Verlag, 1997.
- 71 C. Peter, X. Daura and W. F. van Gunsteren, *J. Biomol. NMR*, 2001, **20**, 297–310.
- 72 D. A. Case, *Acc. Chem. Res.*, 2002, **35**, 325–331.
- 73 P. M. Singer, A. Arsenault, T. Imai and M. Fujita, *Phys. Rev. B*, 2020, **101**, 174508.
- 74 J. Wang, W. Yuan, T. Imai, P. M. Singer, F. Bahrami and F. Tafti, *Phys. Rev. B*, 2021, **103**, 214405.
- 75 T. Imai, P. M. Singer, A. Arsenault and M. Fujita, *J. Phys. Soc. Jap.*, 2021, **90**, 034705.
- 76 E. J. Fordham, L. Venkataramanan, J. Mitchell and A. Valori, *Diffusion Fundam.*, 2017, **29**, 1–8.
- 77 I.-C. Yeh and G. Hummer, *J. Phys. Chem. B*, 2004, **108**, 15873–15879.
- 78 B. Dünweg and K. Kremer, *J. Chem. Phys.*, 1993, **99**, 6983–6997.
- 79 I. Shikhov and C. Arns, *Appl. Magn. Reson.*, 2016, **47**, 1391–1408.
- 80 A. Kalk and H. J. C. Berendsen, *J. Magn. Reson.*, 1976, **24**, 343–366.
- 81 W. A. M. Madhavi, S. Weerasinghe and K. I. Momot, *J. Phys. Chem. B*, 2017, **121**, 10893–10905.